Chapter

Porosity Prediction of a Carbonate Reservoir in Campos Basin Based on the Integration of Seismic Attributes and Well Log Data

Roberta Tomi Mori and Emilson Pereira Leite

Abstract

We have calculated and interpreted a 3D porosity model of a reservoir through the integration of 3D seismic data with geophysical well logs using an artificial neural network (ANN). The reservoir is composed of Albian carbonates. In the first main stage of the study, horizons were traced by following continuous seismic events on seismic sections, along depths between top and base of the reservoir. In the second main stage, predictions of reservoir porosity values were obtained, as well as a 3D model, through the designed ANN. The estimated porosity values range from 5 to 30%. The correlation coefficient and the error of the estimated values with respect to the actual values extracted along the wells are equal to 0.90 and 2.86%, respectively. Porosity values increase from southwest to the northeast portion, and lower values are found at depths related to the traced horizons. Although isolated peaks of maximum porosity are observed, spatial patterns depicted in the model are associated with geological features such as different porosity types and cementation degree.

Keywords: porosity, artificial neural networks, carbonate reservoir

1. Introduction

Reservoir characterization has become increasingly important to hydrocarbon exploration. Accurate characterization reduces the risk of drilling a dry well, as well as exploration and development costs. For this reason, different types of data are used, such as geophysical well logs, and seismic, petrophysical, in addition to geological models, in order to predict reservoir properties such as porosity, lithology, and fluid saturation [1]. In particular, the integration of well logs with seismic data is important in order to obtain some models with better vertical and horizontal resolutions, since well logs have a very restricted area and a better vertical resolution when compared to seismic data; however, seismic data presents a better horizontal resolution and covers a larger area. Integrated quantitative interpretation is used to estimate reservoir properties, obtained through seismic amplitudes and seismic attributes [2–4].

A seismic attribute is any direct or indirect information obtained from the seismic data through mathematical calculation and/or logical reasoning. Depending on how it is derived, an attribute may help the interpreter to delineate geologic structures,

map geologic features, estimate physical properties, etc. [4]. Because each independent attribute provides a particular view of the seismic data, the use of a single attribute leads to a high uncertainty in interpretation [5]. Therefore, the application of multiattribute analysis has grown during the last few decades [2, 6–8]. Multiattribute analysis employs a combination of various seismic attributes through mathematical modeling in order to increase the accuracy in the prediction of a particular property.

In this context, artificial neural networks (ANN) are tools to perform a multiattribute analysis. They allow us to establish a quantitative relationship between the well log data and the seismic data, such that it can be used to predict a physical property in positions where there are no well log data. In general, an ANN is composed of an input layer, an output layer, and one or more intermediate layers that are hidden. In the input layer, there are neurons that represent the input dataset. In the hidden layers, the neurons adjust the input data to the target well log values in the output layer, through an iterative calculation of weights. These weights define the model that is used for prediction of unknown values [3, 7, 9, 10].

In this chapter, we have predicted porosity values of a carbonate reservoir located on Campos Basin through an ANN method, applied to the integration of well log and 3D seismic data. This process provided a 3D numeric volume of porosity of the entire reservoir. We have interpreted the spatial distribution of the porosity values according to geological information obtained from the literature and from descriptions of core samples.

2. Geology of the study area

The Campos Basin is located offshore of the southeastern portion of the Brazilian continental margin (**Figure 1**). It encompasses an area of ~120,000 km^2 and the maximum water depth is ~3400 m. It is limited by the Vitoria Arc on the north, the Cabo Frio Arc on the south, the boundary of the salt diapir region at water depths of ~2200 m on the east, and the updip limits of the turbidites to the west. Campos Fault divides the deepest part (east portion), where cretaceous

Figure 1.
Some of the offshore sedimentary basins of Brazil. Campos Basin is highlighted in red (source accessed in April 2018: http://wdetail.asp?img_id=4775&a_id=117349).

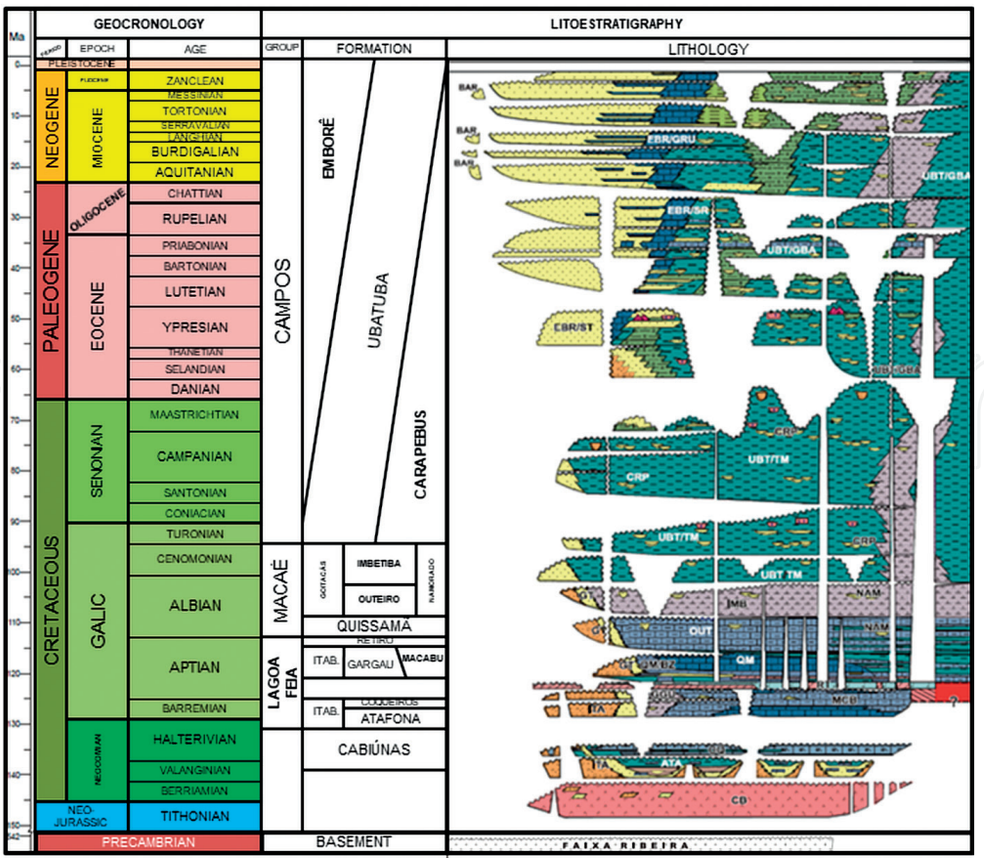

Figure 2.
Simplified stratigraphic column of Campos Basin (adapted from: [12]).

sediments were deposited, from the west portion where the sediments were deposited on top of the basement [11].

The studied reservoir is inserted into the Quissamã formation, which was formed during the final stage of the lower Cretaceous (Albian). This formation is composed of byoncolitic, oolitic, and peloid dolomites, poorly sorted sandstones, polymictic conglomerate associated to calcilutites and marls, and pelitic sediments dominated by marl ([12]; **Figure 2**). Quissamã formation is contained in the Macae Group, which has a shallow carbonate platform dominated by thick shoal carbonates with ooliths and oncolites. The reservoir consists mainly of oncolytic calcarenites and calcirudites, distributed in bars forming a NE trend. It essentially contains microporosity varying between 15 and 30% and has low permeabilities, but the presence of a fracture system contributes to the increasing of permeability in some regions [13].

3. Materials and methods

We have used profiles of neutron porosity, bulk density, gamma ray and sonic travel time from well logs, and a 3D seismic data. P-wave velocity was calculated from sonic logs. HRS (Hampson Russell Software[1]—CGG Veritas) was employed to perform time-depth conversions through seismic-well ties. These tie processes were applied within a time window analysis ranging from the top markers to the base markers. The overall correlation obtained was 0.65, which is not uncommon for this type of application (e.g., [14]).

We then identified continuous reflection events on the seismic sections and defined seismic horizons from the interpolation of picked time/distance pairs. This

[1]http://www.cgg.com/hampson-russell.aspx?cid=3609.

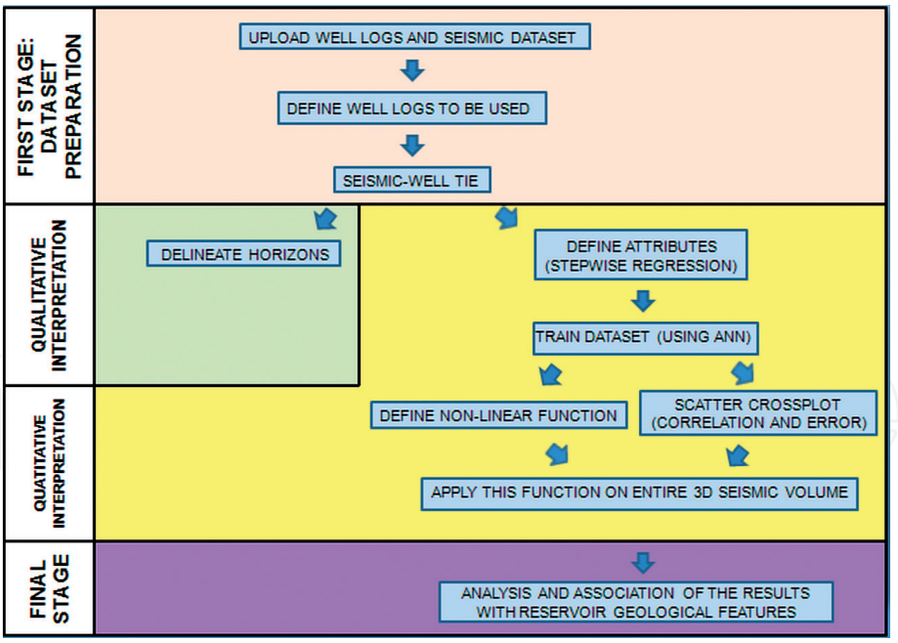

Figure 3.
Flowchart that describes the process applied to obtain our 3D porosity model of the reservoir.

is a qualitative interpretation which does not take into account the seismic amplitude but only the P-wave travel time.

After horizon tracing, we designed and trained an artificial neural network (ANN) to construct a porosity model of the studied reservoir. In the final interpretation stage, we analyzed the results and made the appropriated associations with the geological features found in the literature. These interpretations are also consistent with descriptions of core samples and petrophysical analysis. **Figure 3** shows a simplified scheme of the overall process applied in this work.

3.1 Multiattribute analysis

The general goal of a multiattribute analysis is to find a mathematical relationship between target reservoir properties and seismic attributes. Assuming that seismic-well ties were already conducted, two main stages are necessary to perform a multiattribute analysis (e.g., after this relationship is established along the wells, it is applied to populate the 3D seismic space with the chosen reservoir property (e.g., [9]):

1. To train the seismic attributes along the wells, so that they are mapped onto the desired property space. The most appropriated attributes are defined during this training.

2. To make predictions of the desired property for the entire seismic volume, using the mathematical relationship found on the first stage.

3.2 Probabilistic neural network

In this chapter, we performed a multiattribute analysis using a probabilistic neural network (PNN). This type of ANN has been described, for instance, by Specht [15] and by Masters [16, 17]. It basically consists in an interpolation scheme that uses the architecture of an ANN in its implementation. For example,

consider n training samples where each sample is composed of two input attributes, A_1 and A_2, and one output property value L each, which is the measured target log value. In matrix form, this training set is a $n \times 3$ matrix whose entries are $\{A_{1i}, A_{2i}, L_i\}$ where $i = 1, \ldots n$.

A PNN assumes that each new output value can be described as a linear combination of the input values in the training set. For a new input sample, $x = \{A_{1j}, A_{2j}\}$; an output value $L'(x)$ is estimated as

$$L'(x) = \frac{\sum_{i=1}^{n} L_i \exp(-D(x, x_i))}{\sum_{i=1}^{n} \exp(-D(x, x_i))}, \quad (1)$$

where

$$D(x, x_i) = \sum_{i=1}^{2} \left[\frac{x_j - x_{ij}}{\sigma_j}\right]^2. \quad (2)$$

$D(x, x_i)$ is the distance between the input data and each training point x_i (**Figures 4** and **5**). This distance is measured in a multidimensional attribute space and normalized by the quantity σ_j [2].

The PNN training consists in determining the best group of smoothing parameters σ_j. The criterion used to determine these parameters is a minimum validation error [2].

The validation result for the mth target sample is defined as

$$L'(x_m) = \frac{\sum_{i \neq m} L_i \exp(-D(x_m, x_i))}{\sum_{i \neq m}^{n} \exp(-D(x_m, x_i))}. \quad (3)$$

This is the predicted value of the mth target sample when this sample is left out of the training dataset. In other words, this means that the dataset is trained without that sample. By repeating this process for each training sample, total prediction error can be defined as

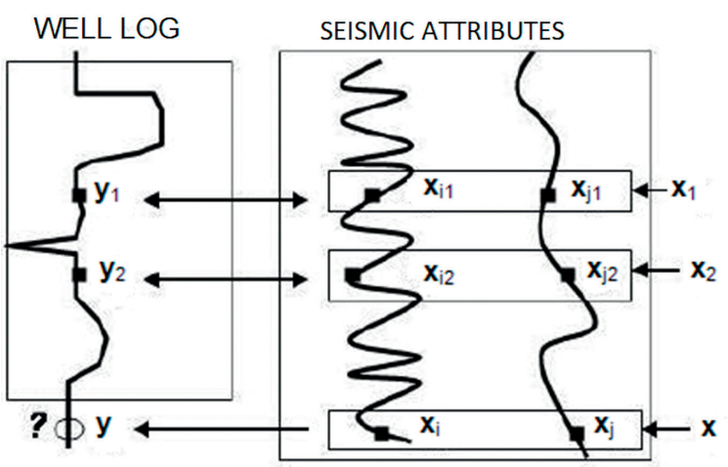

Figure 4.
Representation of the positions at which the input vectors (x_1 and x_2) are associated to known target values of an output vector (y_1 and y_2) and a position where an input vector (x) is associated to an unknown target value of an output vector (extracted from [5]).

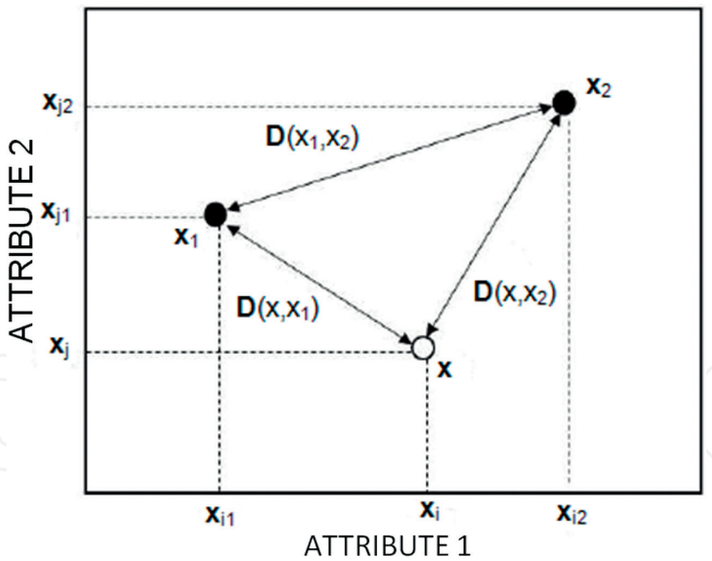

Figure 5.
Schematic graph of vectors x_1, x_2, and x, relative to **Figure 4** *where the coordinate axes represent the attribute amplitudes instead of Cartesian distances (modified from [5]).*

$$E(\sigma_1, \sigma_2, \sigma_3) = \sum_{i=1}^{N} \left(L_i - L'_i\right)^2. \quad (4)$$

4. Results and discussion

We have defined four horizons that were delineated by tracking continuous seismic events (**Figure 6**). The deepest one (**Figure 6a**) represents the reservoir base, while the shallowest (**Figure 6d**) represents the reservoir top. Between these horizons, there are more two horizons, termed intermediate horizons (**Figure 6c** and **d**). Drill core data show carbonate textures such as packstones and wackestones at depths near these horizons. These textures are composed by rock matrices rich in carbonate, which explains the decrease of porosity in these regions.

The PNN method was applied in the interval between the reservoir base and top horizons. After the training process, we have obtained a seismic attribute list that yields the highest correlation between predicted porosity and actual porosity at the wells and the lowest prediction error, through a stepwise regression. The attribute list and the total training error are presented in **Table 1**.

Then, using this attribute list, we applied the training process through the PNN using 12–19 attributes. Each training result was analyzed based on a correlation coefficient and a training error (**Figure 7b** and **c**). Based on the correlation and error values, 17–19 attributes yield the best predictions. Therefore, we chose the minimum number of attributes that produces the highest correlation and the lowest error. The prediction power of the trained PNN can be observed in the scatter plot of **Figure 7a**. The correlation coefficient is ~0.9 and the fitting error is ~2.86.

The trained PNN was applied to predict porosity values in the entire 3D seismic volume. **Figures 8a**, **b and 9a–d** show the porosity distribution along vertical and time slices extracted from the 3D porosity model. The spatial distribution of this model can also be observed in **Figure 9e** and **f**.

This model shows high heterogeneity in the distribution of the predicted porosity values, which vary from 5 to 30%, with an average of around 19%. These values

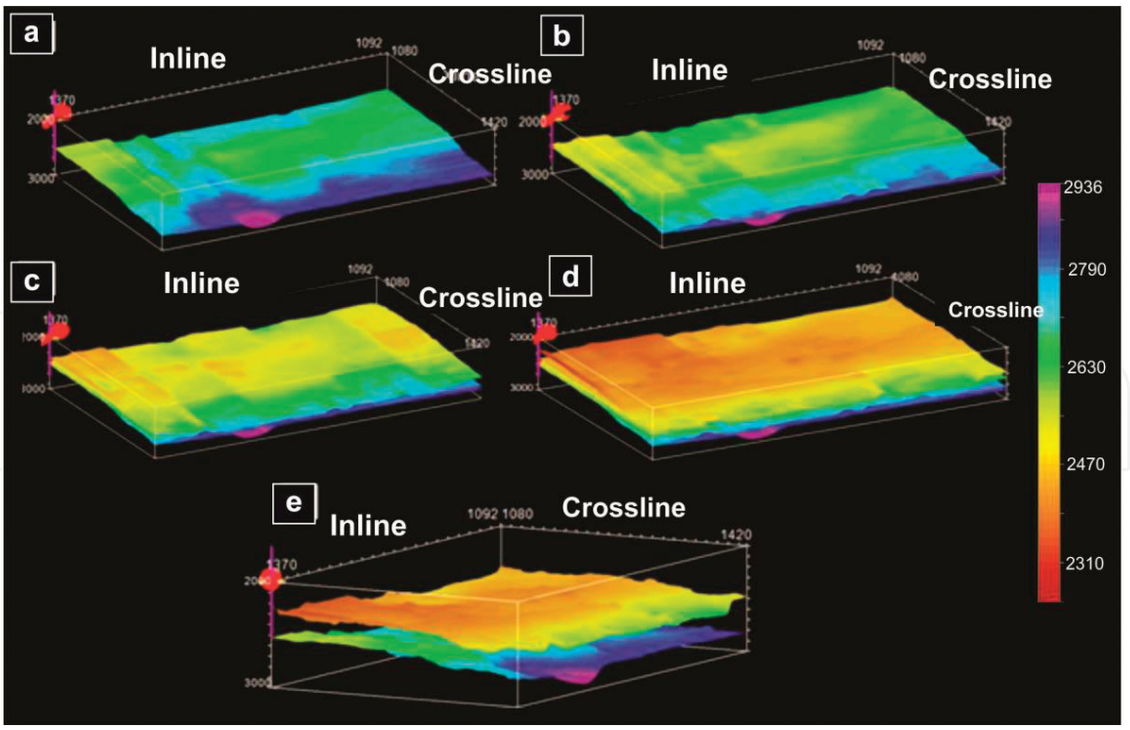

Figure 6.
(a) Deepest horizons representing reservoir base, (b) deepest intermediate horizon, (c) the shallowest intermediate horizon, (d) the shallowest horizon representing reservoir top, and (e) reservoir top and base horizons.

	Target log	Attribute	Training error
1	Porosity	Dominant frequency	6.066539
2	Porosity	Amplitude weighted phase	5.847074
3	Porosity	Average frequency	5.770756
4	Porosity	Integrated absolute amplitude	5.677001
5	Porosity	Apparent polarity	5.634725
6	Porosity	Instantaneous frequency	5.595683
7	Porosity	Amplitude weighted cosine phase	5.577585
8	Porosity	Amplitude envelope	5.552585
9	Porosity	Amplitude weighted frequency	5.512237
10	Porosity	Quadrature trace	5.496368
11	Porosity	Instantaneous phase	5.484175
12	Porosity	Cosine instantaneous phase	5.454468
13	Porosity	Second derivative instantaneous amplitude	5.441876
14	Porosity	Filter 5/10–15/20	5.432924
15	Porosity	Filter 15/20–25/30	5.423227
16	Porosity	Integrate	5.414948
17	Porosity	Filter 25/30–35/40	5.409717
18	Porosity	Second derivative	5.407269
19	Porosity	Derivative	5.407243

Table 1.
Attribute list obtained after training with PNN and stepwise regression.

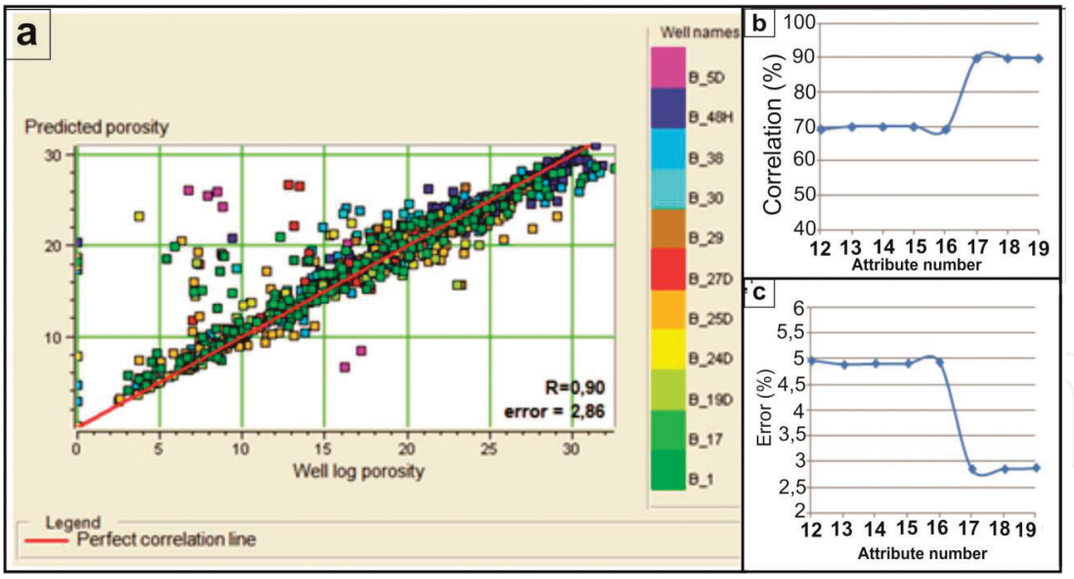

Figure 7.
(a) Correlation between predicted porosity and well log porosity and the errors related to this correlation, obtained by probabilistic ANN. (b) Correlation between predicted porosity and actual porosity of PNN training using 12–19 attributes. (c) PNN training error.

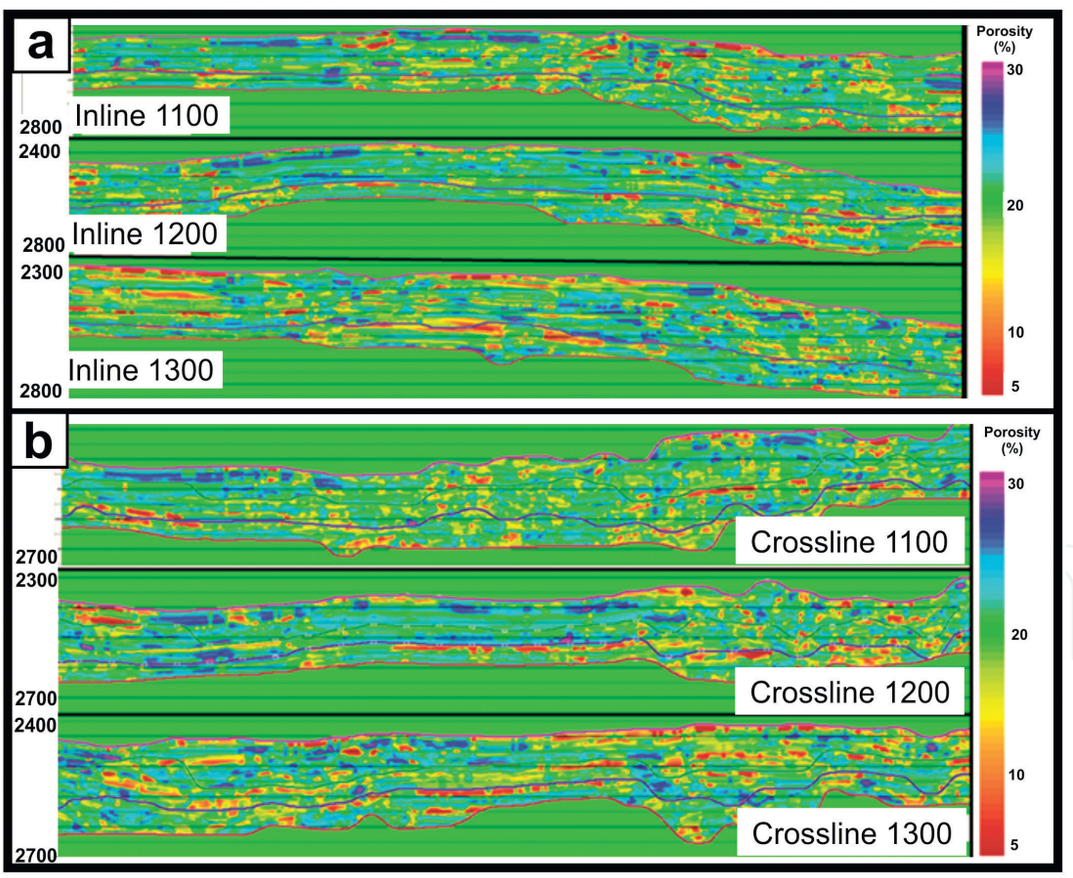

Figure 8.
(a) Predicted porosity obtained by a PNN along inlines 1100, 1200, and 1300. (b) Predicted porosity obtained by a PNN along crosslines 1100, 1200, and 1300.

increase from south to north and from west to east, with the highest values occurring on the northeast and on the central portion. Besides the horizontal porosity variation, we can also observe a significant vertical variation, in which the highest values are concentrated on the intermediate depths of reservoir, and there is also a decrease

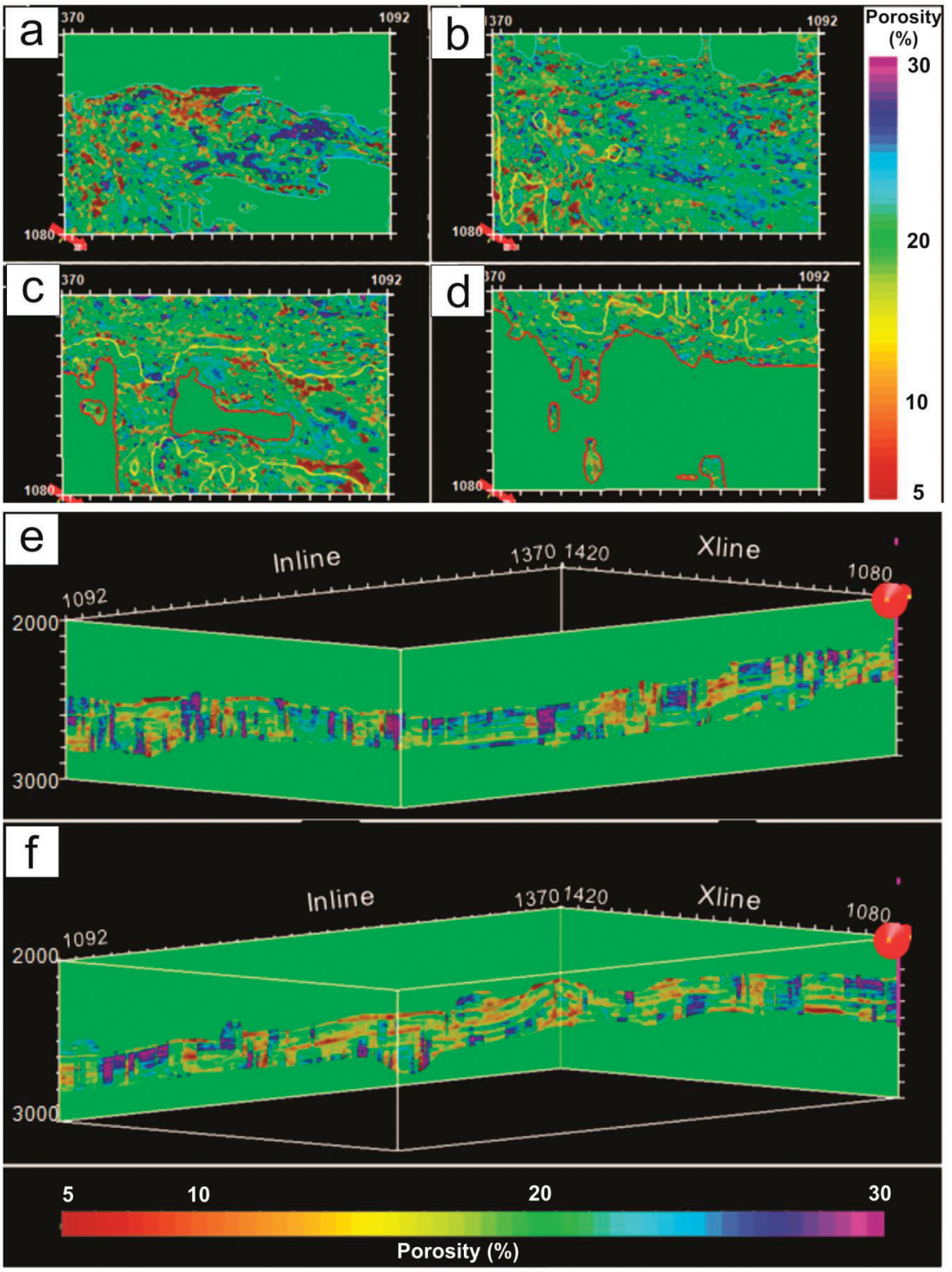

Figure 9.
(a) A plan view of predicted porosity obtained by probabilistic ANN in 2400 ms, with north pointing to the bottom right corner of the image. (b) Predicted porosity in 2500 ms. (c) Predicted porosity in 2600 ms. (d) Predicted porosity in 2700 ms. (e) 3D volume of predicted porosity obtained by probabilistic ANN, on inline 1092 and crossline 1080. (f) 3D volume of predicted porosity on inline 1370 and crossline 1420.

on these values on depths corresponding to the interpreted seismic horizons. Based on this information, we could identify three different groups of porosity: (1) those with low values (5–10%) and concentrated on the southwest portion and near seismic horizons; (2) those with intermediate values (10–22%) and dispersed in the entire seismic volume, however concentrating more on the northeast and on the central portion; and (3) those with high values (22–30%) concentrated in some specific regions, mostly on the northeast and on the central portion.

Melani [13] explains the difference between the porosity values on the northeast portion and on the southwest portion as the result of different porosity types. On the northeast, the porosity is the original macroporosity of the rocks, while in the southwest it is essentially microporosity. Besides this noticeable division, according to petrophysical and drill core data, porosity values vary due to rock texture variation of reservoir carbonates. Grainstones are related to higher porosity values, while packstones and wackestones are related to lower values, because of the difference in the degree of cementation.

Furthermore, the lower porosity values near the seismic horizons can be related to a higher cementation degree in these regions, where rock textures vary from packstone to wackestone. The variation of cementation degree occurred because of different energy availability in the depositional environment, which corresponds to drowning and shallowing cycles on these regions.

5. Conclusions

We have created a 3D porosity model of a carbonate reservoir in the Campos Basin through the application of a PNN that integrates well logs and seismic data. The overall correlation between predicted and actual porosity values is ~0.90, while the training error is ~2.86. This model presents high spatial heterogeneity. In general, porosity values increase from southwest to northeast, and the highest concentration is located on the northeast and central areas. This is explained by different porosity types in the reservoir, where the higher values are concentrated in regions where the original macroporosity was preserved and the lower values are concentrated where the porosity is classified as microporosity. While the shallowest horizon is related to the reservoir top and the deepest is related to the reservoir bottom, the two intermediate horizons are related to discontinuities with different cementation degrees. These horizons are associated to different rock textures caused by energy availability variation in the depositional environment. Our interpretations are based on petrophysical and drill core data available in the published literature.

Acknowledgements

The authors thank the Institute of Geosciences at the University of Campinas for providing all resources to the development of this work. This study was financed in part by the Coordenação de Aperfeiçoamento de Pessoal de Nível Superior—Brasil (CAPES)—Finance Code 001, for which Roberta Tomi Mori is grateful for her Masters scholarship. Emilson Pereira Leite thanks Conselho Nacional de Desenvolvimento Científico e Tecnológico (CNPq) for his Productivity Grant #301593/2012-4.

DOI: http://dx.doi.org/10.5772/intechopen.82490

IntechOpen

Author details

Roberta Tomi Mori and Emilson Pereira Leite*
Department of Geology and Natural Resources, Institute of Geosciences, University of Campinas, Campinas, SP, Brazil

*Address all correspondence to: emilson@ige.unicamp.br

References

[1] Mohaghegh S, Arefi R, Ameri S, Aminiand K, Nutter R. Petroleum reservoir characterization with the aid of artificial neural networks. Journal of Petroleum Science and Engineering. 1996;**16**:263-274

[2] Hampson D, Schuelke J, Quirein J. Use of multi-attribute transforms to predict log properties from seismic data. Geophysics. 2001;**66**:220-236

[3] Leite EP, Vidal AC. 3D porosity prediction from seismic inversion and neural networks. Computers & Geosciences. 2011;**37**:1174-1180

[4] Taner MT. Seismic attributes. CSEG Recorder. 2001;**26**(7):49-56

[5] Russell BH. The application of multivariate statistics and neural networks to the prediction of reservoir parameters using seismic attributes [PhD thesis]. Canada: University of Calgary; 2004. 392p

[6] Brown AR. Understanding seismic attributes. Society of Exploration Geophysicists. 2001;**66**(1):47

[7] Khoshdel H, Riahi MA. Multi attribute transform and neural network in porosity estimation of an offshore oil field—A case study. Journal of Petroleum Science and Engennering. 2011;**78**:740-747

[8] Taner MT, Walls J, Taylor G. Seismic attributes, their use in petrophysical classification. In: EAGE 63° Conference & Technical Exhibition—Amsterdam, The Netherlands; 2001

[9] Schultz PS, Ronen S, Hattori M, Corbett C. Seismic guided estimation of log properties, parts 1, 2, e 3. The Leading Edge. 1994;**13**:305-310, 674-678, and 770-776

[10] Valenti JCAF. Porosity prediction from seismic data using multiattribute transformations, N sand, Auger Field, Gulf of Mexico [Master thesis]. United States: The Pennsylvania State University; 2009. 84p

[11] Guardado LR, Gamboa LAP, Lucchesi CF. Petroleum geology of the Campos Basin: A model for producing Atlantic type basin. In: Edwards JD, Santogrossi PA, editors. United States: Divergent/Passive Margin Basins. Vol. 48. AAPG Memoir; 1989. pp. 3-79

[12] Winter WR, Jahnert RJ, França AB. Bacia de Campos. Boletim de Geociências da Petrobras, Rio de Janeiro. 2007;**15**:511-529

[13] Melani LH. Caracterização petrofísica de reservatório carbonático [Dissertação de Mestrado]. Campinas: Faculdade de Engenharia Mecânica e Instituto de Geociências, Universidade Estadual de Campinas; 2015. 80p

[14] Sancevero SS, Remacre AZ, Portugal RS. O papel da inversão para a impedância acústica no processo de caracterizacão sísmica de reservatórios. Revista Brasileira de Geofísica. 2006;**24**(4):495-512

[15] Specht DF. Probabilistic neural networks. Neural Networks. 1990;**3**(1):109-118

[16] Masters T. Practical Neural Network Recipes in C++. United States: Academic Press, Inc; 1993

[17] Masters T. Advanced Algorithms for Neural Networks. United States: John Wiley & Sons, Inc; 1995